Sensitivity analysis of thermophysical properties on PCM selection under steady and fluctuating heat sources: A comparative study

Xiaoli Yu [a,b], Jinwei Chang [a], Rui Huang [a,b], Yan Huang [a], Yiji Lu [a,c], Zhi Li [a,*], Lei Wang [a,d,*]

[a] *Department of Energy Engineering, Zhejiang University, Hangzhou, 310027, P.R. China*

[b] *Ningbo Research Institute, Zhejiang University, Ningbo, 315100, P.R. China*

[c] *Durham Energy Institute, Durham University, Durham, DH1 3LE, The United Kingdom*

[d] *Ningbo C.S.I Power & Machinery Group Co., Ltd., Ningbo, 315020, P.R. China*

HIGHLIGHTS

- Effects of PCM thermophysical properties on LTES performance are investigated
- Prominent factors for PCM selection under different conditions are specified
- PCM selection for LTES under fluctuating heat source condition is studied
- The effect of C_p and L on charging rate is reinforced under fluctuating heat source
- $LiNO_3$-$NaNO_2$ performs the best under both steady and fluctuating heat sources

Abstract

Previous studies on phase change material (PCM) selection for latent thermal energy storage (LTES) mainly focused on steady heat source conditions without considering the effects of thermal fluctuation of real heat sources, and how fluctuating heat sources will affect the charging performance of LTES and material selection is still unclear. This study aims to compare the difference in material selection for a shell-and-tube LTES under steady and fluctuating heat sources,

Email address: liz_ym@zju.edu.cn *(Z. Li)*

wanglei@ningdong.com *(L. Wang)*

which comprehensively considers the effects of PCM thermophysical properties including the melting temperature, density, specific heat capacity, thermal conductivity and latent heat, as well as their interaction effects. By taking heat storage capacity and charging rate as objectives, orthogonal experiment design and stepwise regression analysis have been conducted to specify the significant factors among these parameters under steady and fluctuating heat source conditions. To further investigate the difference in the ranking of candidate PCMs under two conditions, fourteen pre-screened PCMs are ranked under steady and fluctuating heat sources. The results show that the order of prominent factors for heat storage capacity is $\rho \cdot C_p$, followed by $\rho \cdot L$ under both conditions. However, when considering the charging rate, temperature fluctuation will weaken the effect of melting temperature, and strengthen the effect of specific heat capacity and latent heat. The order of prominent factors for charging rate is $\lambda \cdot C_p$ and $C_p \cdot L$ under fluctuating heat source. According to the ranking results, $LiNO_3$-$NaNO_2$ within the melting temperature of 100-200 ℃ has an excellent comprehensive charging performance under both conditions.

***Keywords*:** Latent thermal energy storage, Phase change materials, Multi-criteria decision, Fluctuating heat source, PCM selection

Nomenclature

A_{mush}	Porosity function in momentum equations (kg/m^3 s)
C	Constant coefficient of porosity function (kg/m^3 s)
C_p	Specific heat capacity (J/kg K)
e	The indicator after range normalization
f	Liquid fraction
H	Enthalpy of the PCM (kJ/kg)
h	Heat transfer convection coefficient (W/m^2 K)
K	Thermal conductivity (W/m K)
L	Latent heat of PCM (kJ/kg)
l	Length (mm)
Q	Heat storage capacity (kJ)
q	Sensible heat of PCM (kJ)
R_Q	Range of heat storage capacity (kJ)
R_V	Range of charging rate (kJ/s)
r_1	Inner radius of the tube (m)
r_2	Inner radius of the shell side (m)
T	Temperature (°C)
t	Time (s)
V	Charging rate (kJ/s)

Greek letters

α	Volumetric expansion coefficient (1/K)
β	Local liquid fraction
ρ	Density (kg/m^3)
λ	Thermal conductivity of PCM (W/m K)
μ	Dynamic viscosity (Pa·s)
ε	Constant number

Subscript

m	Melting
$HTF\text{-}us$	Heat transfer fluid under fluctuating heat source condition
$HTF\text{-}s$	Heat transfer fluid under steady heat source condition
F	Heat transfer fluid
us	Fluctuating heat source condition
s	Steady heat source condition
p	Predicted
ref	Reference

Abbreviations

HTF	Heat transfer fluid
LTES	Latent heat thermal energy storage
ORC	Organic Rankine Cycle
PCM	Phase change material
WHR	Waste heat recovery
MCDM	Multiple Criteria Decision Making
TOPSIS	Techniques for Order Preference by Similarity to Ideal Solutions
Rs	The ranking under steady heat source condition
Rf	The ranking under fluctuating heat source condition

1. Introduction

The nature of intermittent and fluctuating thermal sources such as solar, geothermal and industrial waste heat is one of the key research challenges in the development of thermal energy conversion and storage technologies [1-3]. Latent thermal energy storage (LTES) using phase change material (PCM) is a promising solution to minimize the negative effect from fluctuating heat sources [4, 5]. In such a system, LTES using PCM firstly absorbs heat from the heat transfer fluid (HTF) with fluctuating mass flow rate and temperature and then releases the stored heat to waste heat recovery (WHR) systems.

With the advantage of PCM having large enthalpy of fusion, this technology has been widely studied in the applications of the solar energy and industrial waste heat. Esen [6] investigated a cylindrical phase change material tank combined with a solar-powered heat pump system by a theoretical model, and the storage can help the heat pump operate at a higher coefficient of performance. Faegh et al. [7] proposed an innovative system using in combination with PCM for desalination. The PCM can recover the latent heat of condensing vapor in solar stills and therefore the waste heat can be stored to recycle. The results demonstrated that the PCM-based solar still can improve the water yield by 86%. Furthermore, Organic Rankine cycle (ORC) system is playing an important role in WHR [8, 9], and ORC integrated with LTES can have great potential of energy saving. Cioccolanti et al. [10] proposed a new small scale concentrated solar ORC using PCM for thermal storage and evaluated the performance of the integrated system by simulation. They have found that high annual operating hours, power production and conversion efficiencies can be achieved by using PCM for storing heat. Dal Magro et al. [11] studied an ORC system combined with a PCM-based technology in steel billet reheating furnace and the results showed that the PCM-based technology allowed an increase of capacity factor by 14% and average thermal efficiency improvement almost by 1%.

It can be seen that the heat recovery systems integrated with LTES are recognized as an effective way to address the fluctuation of thermal energy and improve energy efficiency. In order to promote the performance of PCM as retrofit

in LTES system, much research has focused on studying the design parameters of LTES system in recent years. Esen et al. [12] compared and investigated the performance of a solar assisted cylindrical energy storage tank with different PCMs. The authors suggested that PCM, cylinder radius, and the inlet temperature and mass flow of HTF can affect the performance of the storage and should be chosen carefully when optimizing the performance. Nie et al. [13] studied the effect of geometry on the performance of the shell-and-tube latent thermal energy storages using pure PCM and composite PCM. The results revealed that the impact of geometry modification on the thermal performance is different with pure and composite PCMs. Compared with cylindrical unit with copper foam of 94.86% porosity, the optimum angle of frustum tube in value with 2° can make complete melting time decrease by 5.9%. And some research [14] have revealed that the PCM melting process depend on not only geometric parameters, but the thermophysical properties of PCM. In fact, different PCMs on account of distinctive properties will take effects on the overall charging performance of LTES. Therefore, it is critical to select an optimal PCM for an exceptional storing performance during the initial phase of the design of LTES system. As for the PCM selection for LTES, the melting temperature of PCMs should be qualified within the operating temperature first. Then the relative importance of the thermophysical properties of PCM will be assessed according to the requirements of specific applications [15]. Thus, the PCM selection criteria for LTES depends on the purpose of real applications. Regarding the fields of solar energy and industrial waste heat recovery, PCM should have great charging performance [16, 17]. The definition of a LTES with excellent performance means the system possesses large heat storage capacity and high charging rate during the charging process. However, these two indicators are generally contradictory [18]. Therefore, PCMs for LTES system need to be carefully selected based on the actual requirements.

In fact, PCM selection has been widely discussed in the low-and-medium temperature WHR fields in recent years. For example, Loganathan et al. [19] selected a suitable PCM for thermal management power electronic devices by using the criterial weights of Fuzzy Analytical Hierarchy Process. And this study regarded the melting temperature and latent heat as the most important two factors while selecting. Rastogi et al. [20] aimed to select PCM for keeping the suitable

room temperature using LTES, taking two Figures of Merit (FOMs) as objectives, which are $FOM_1=\rho \cdot L$ and $FOM_2=\lambda/(\rho \cdot Cp)$, representing the heat storage capacity and the heat energy transfer rate respectively. The selected optimal PCM can effectively keep the room temperature within the human comfort zone from 21 ℃ to 26 ℃. Tang et al. [21] proposed a practical ranking system to assess superior PCMs for use in buildings. In this analysis, latent heat, melting temperature and thermal conductivity are chosen as evaluation indicators for thermal performance. Above studies demonstrated that a suitable material for buildings and thermal management applications can be fabricated within the desired operating temperature range and have a high latent heat of fusion. But selecting PCM for the higher melting temperature of PCM applications has been paid little attention.

In the WHR applications using medium-to-high temperature PCMs, Xu et al. [15] employed the Analytical Hierarchy Process (AHP), which subjectively employed weights of density, latent heat, specific heat capacity, cost, and thermal conductivity in a case study of using LTES system in a cogeneration plant. Then Techniques for Order Preference by Similarity to Ideal Solutions (TOPSIS) method was adopted to rank the candidate PCMs with phase change temperature between 200 ℃ and 350 ℃. Yang et al. [22] combined AHP with the entropy information method taking into account the subjective and objective weighting of the criteria to rank materials used in ground source heat pump integrated with phase change thermal storage system. However, the effect of the PCM melting temperature was not included during the selection process above the two studies. In fact, the melting temperature of PCM can influence the performance of LTES. Li et al. [23] investigated the thermal performance of a solar chimney with PCM and found that phase change temperature greatly influenced the charging rate. For example, when the phase change temperature is decreased by 10 °C, the melt-down time will reduce by almost 50%. Tao et al. [24] revealed the effects of thermophysical properties of molten salt PCM on the heat and exergy storage performance of a shell-and-tube LTES unit. It was found that PCM with a lower melting temperature is beneficial to the improvement of the charging rate and heat storage quality. In summary, when the temperature difference between the heat source and melting temperature of PCM is relatively large, especially for a wider melting temperature range of candidate PCMs, the influence of melting temperature on

charging process should be considered while selecting proper PCMs.

Meanwhile, waste heat sources with the nature of intermittence and fluctuation in the actual situations, therefore, the heat transfer process of LTES was also investigated under fluctuating heat sources. Huo et al. [25] proposed the heating method which was simplified as time-variant heat flux with square wave for a LTES tank and numerically studied the effects of periods and amplifications for the PCM melting process. The results showed that fluctuating heat flux could reduce the final average temperature and melting time of PCM compared with steady-state heat boundary. Li et al. [26, 27] investigated the dynamic heat transfer characteristics of LTES and the effects of the composite PCM with Al_2O_3 nanoparticles and pure PCM on the melting process under different sinusoidal fluctuating heat sources. It was found that fluctuating heat sources with large fluctuation can significantly accelerate the melting rate and decrease the energy storage capacity of LTES in comparison with the constant heat source. The total melting time and energy storage capacity are reduced by 24.5% and 9.5% when the fluctuating period is 60 min in contrast to that of the constant heat source. The reviewed literature demonstrated that the fluctuation of heat source could bring about a great effect on the charging performance of LTES. It can be inferred that the existing of fluctuating heat sources might lead to the different results of material selection compared with steady heat sources.

Based on the above literature, it can be concluded that the effects of thermophysical properties on the PCM selecting process have not been completely revealed on the one hand. For example, the impact of the melting temperature of PCMs on charging performance was less considered in the WHR applications when conducting the PCM selection process, and the correlation effects among thermophysical properties of PCM are still unclear, including thermal conductivity, density, specific heat capacity, melting temperature and latent heat. On the other hand, previous studies have not dealt with the difference in PCM selection between the steady and fluctuating heat sources, and it is an urgent need to understand the effects of thermal fluctuations on the material selection because most of the real heat sources are fluctuating and intermittent. Therefore, this study aims to reveal the difference in PCM selection for a shell-and-tube LTES under steady and fluctuating heat sources, comprehensively considering the effects of thermophysical properties

and their interaction. Taking heat storage capacity and charging rate as the objectives of charging performance, the influence of PCM thermophysical properties is analysed by orthogonal design and stepwise regression analysis. Then, common actual materials are taken as an example to examine the difference of ranking under steady and fluctuating conditions. The ranking results obtained by TOPSIS method are validated by pareto solution and simulation, and a sensitivity analysis is also conducted by applying varied weightings to objectives. The results of this study can provide new insights into the influence of heat source fluctuation on the material selection, and benefit the design and optimization of PCM in a shell-and-tube LTES for fluctuating heat source in the future.

2. Methodology

To identify the difference in PCM selection between steady and fluctuating heat source conditions, the main methodology adopted in the current study is firstly introduced. Then, the potential PCMs are selected and pre-screened in terms of the operating conditions and applications of the LTES system. Finally, the simulation model of a shell-and-tube LTES heat exchanger was illustrated and validated, and the simulation model would be employed to the following study.

2.1 Selection procedure of phase change material

This work aims to investigate the difference in PCM selection for a shell-and-tube LTES between steady and fluctuating heat source conditions. In the present study, the heat storage capacity and charging rate are used as the key objectives to assess the charging performance of the LTES system during the selecting process. Besides, the following study of the influence of PCM thermophysical properties on LTES performance is explored through the simulation method, and the simulation model is described in detail in Section 2.3. Compared with the inlet temperature fluctuation, the effects of HTF flow rate fluctuation have negligible impacts on the thermal energy storage performance as reported by references [28, 29]. Therefore, the fluctuating heat source condition only considers the temperature fluctuation without giving considerable attention to the mass flow rate change of HTF in this research. Meanwhile, research shows

that natural convection could significantly accelerate the PCM charging process [30, 31], so natural convection is considered in this work to ensure the reliability of the results.

The flowchart shown in **Fig. 1** illustrates the selection procedure of PCM under steady and fluctuating heat source conditions. Based on the operating conditions and applications of the LTES system, potential candidates are pre-screened by primarily considering the range of melting temperature and availability of the phase change materials. Then, an orthogonal experiment with 5 test factors and 4 levels is designed to do an initial analysis of specifying the difference in single-factor effects between steady and fluctuating heat source conditions. Next, the stepwise regression analysis has been conducted to analyse the interaction effects among PCM thermophysical properties on the heat storage capacity and charging rate. The relationships between these two key objectives and the five thermophysical properties of PCM are represented as multiple nonlinear regression equations using the uniform experiment design method and regression analysis. The obtained equations are applied to predict the charging performance of the actual materials later. The results are used to provide a ranking through TOPSIS method, which is an efficient ranking method developed by Hwang and Yoon [32]. The obtained results are compared to the results from the Pareto front method and simulation to demonstrate the accuracy. Besides, the differences in the charging performance of actual PCMs between the two conditions are analysed. Finally, a sensitivity analysis is conducted by applying various weightings to objective functions.

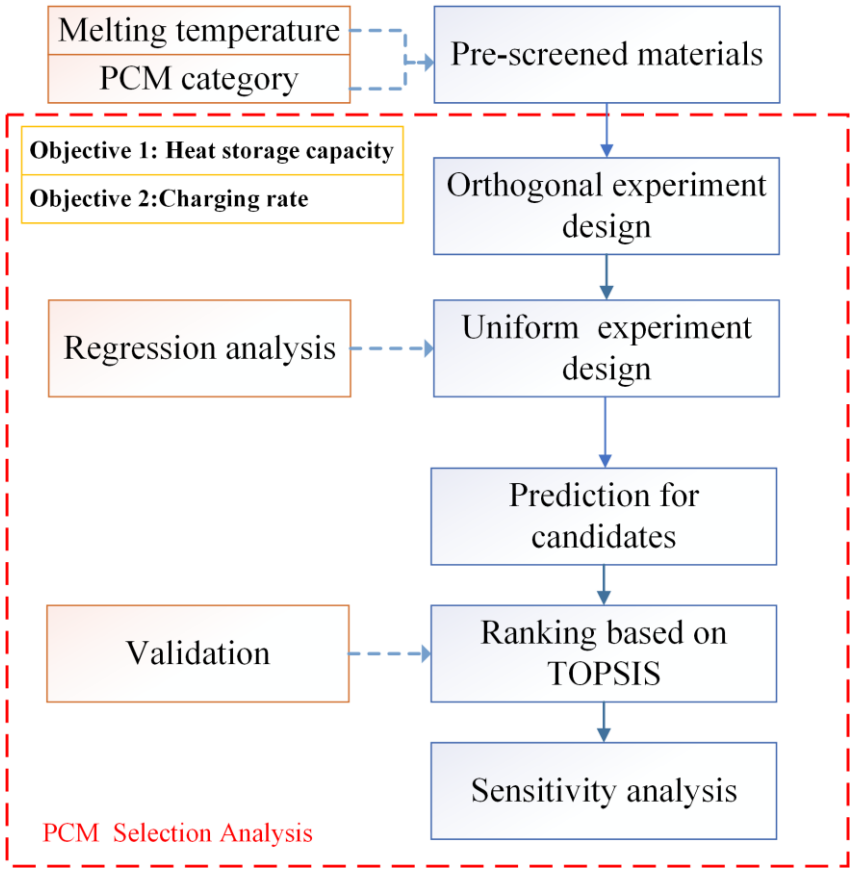

Fig. 1. Flowchart of the material selection analysis under steady and fluctuating heat source conditions.

2.2 Pre-screening of phase change materials

Phase change materials such as organic materials, salt and salt composite have been widely used in the LTES systems [33, 34], due to the relatively large latent heat, adjustable melting temperature and low cost. The pre-selection principle in this work is focused on the range of heat source temperature (200-400 ℃) and the operating temperature of the WHR system, such as the Organic Rankine cycle. Therefore, some commonly used salts/salt composites and promising organic PCM are included in a preferred consideration list. In this paper, fourteen popular phase change materials with melting temperature in the range of 100-200 ℃ from Ref. [35] are pre-screened to study and the detailed information is shown in **Table 1**.

Table 1 Thermophysical properties of selected Phase Change Materials [35].

NO.	Candidates	Mass ratio	T_m	ρ	L	C_p	λ
			℃	kg/m^3	kJ/kg	J/(kg·K)	W/(m·K)
1	KNO_3-$LiNO_3$-$NaNO_3$	52:30:18	123	2068	140	1440	0.53
2	$LiNO_3$-KNO_3	34:66	133	2018	150	1350	0.52
3	KNO_3-$NaNO_2$	56:44	141	1994	97	1740	0.57
4	KNO_3-$NaNO_3$-$NaNO_2$	53:6:41	142	2006	110	1730	0.57
5	KNO_2-$NaNO_3$	48:52	149	2080	124	1630	0.52
6	$LiNO_3$-$NaNO_2$	62:38	156	2296	233	1910	0.66
7	$LiNO_3$-$NaNO_3$-KCL	45:50:5	160	2297	266	1690	0.59
8	$LiNO_3$-KCl	58:42	160	2196	272	1350	0.59
9	HDPE		130	952	255	2150	0.44
10	Urea		134	1320	250	2110	0.60
11	HCOONa–HCOOK	45:55	176	1913	175	930	0.43
12	Urea–NH_4Cl	85:15	102	1348	214	2090	0.58
13	Urea–NaCl	90:10	112	1372	230	2020	0.60
14	Urea–K_2CO_3	15:85	102	1415	206	2020	0.58

2.3 Simulation model of a shell-and-tube latent thermal energy storage

The schematic diagram of a shell-and-tube LTES heat exchanger is shown in **Fig. 2**. The PCM placed in the outer layer absorbs the heat released from HTF flowing through the inside. The geometric parameters are defined as follows: the length of the LTES heat exchanger (l) is 1000 mm, and the radius of the inner tube (r_1) and outer shell (r_2) are 12.5 mm and 25 mm, respectively. And the inlet temperature of HTF is set at $T_{HTF,s}$=300 ℃ for steady heat source, while fluctuating heat source is assumed as a sinusoidal fluctuation $T_{HTF,us}$=100·sin(πt/1800) +300 ℃. To simplify the mathematical model, the following assumptions are adopted:

(1) The thickness of the tube wall is not considered;

(2) The thermophysical properties of PCM and HTF are independent of temperature except the density of PCM;

(3) The axial heat conduction and viscous dissipation in the HTF is neglected and the HTF flow is treated as one-dimensional fluid flow;

(4) Due to the symmetry, half of the tube is chosen as the computational domain and with consideration of natural convection, a two-dimensional cross-section of PCM is selected.

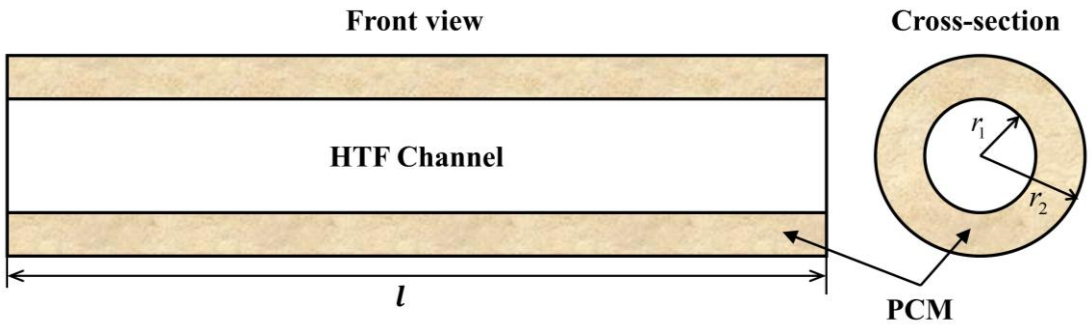

Fig. 2. Schematic diagram of the shell-and-tube LTES heat exchanger.

2.3.1 Governing equations

A two-dimensional (2-D) transient heat transfer model for the cross-section of a shell-and-tube LTES unit based on the enthalpy method is presented to simulate the moving boundary problem within the PCM. Firstly, the continuity equation for PCM is written as follows:

$$\frac{\partial \rho}{\partial t} + \frac{\partial (\rho u)}{\partial x} + \frac{\partial (\rho v)}{\partial y} = 0 \tag{1}$$

In the enthalpy method, liquid state and solid state have the same form of the energy equation. The solid-liquid interface is indicated as a mushy zone to separate two phases. The energy equation for PCM can be described as:

$$\frac{\partial \rho H}{\partial t} + \frac{\partial (\rho u H)}{\partial x} + \frac{\partial (\rho v H)}{\partial y} = \frac{\partial}{\partial x}\left(k \frac{\partial T}{\partial x}\right) + \frac{\partial}{\partial y}\left(k \frac{\partial T}{\partial y}\right) \tag{2}$$

Where H represents the total enthalpy of sensible enthalpy and latent enthalpy, which can be calculated by Eq. (3) and (4). q_{ref} denotes the sensible enthalpy at the reference temperature T_{ref}.

$$H = q + f \cdot L \tag{3}$$

$$q = q_{ref} + \int_{T_{ref}}^{T} C_p dT \tag{4}$$

Where f refers to the liquid volume fraction (the ratio of liquid PCM volume to the total volume of computational cell) calculated by Eq. (5).

$$f=\begin{cases}0 & T<T_{solidus}\\ \dfrac{T-T_{solidus}}{T_{liquidus}-T_{solidus}} & T_{solidus}\le T\le T_{liquidus}\\ f=1 & T>T_{liquidus}\end{cases} \tag{5}$$

200 Substituting Eq. (3) -(5) into Eq. (2), the energy equation can then be written as:

$$\frac{\partial \rho h}{\partial t}+\nabla\cdot\left(\rho v h\right)=\nabla\cdot\left(k\nabla T\right)-\frac{\partial \rho fL}{\partial t}-\nabla\cdot\left(\rho v fL\right) \tag{6}$$

201 The existence of natural convection will promote the increase of sensible heat and accelerate the melting process
202 [36]. With consideration of the small variation in density, the natural convection is taken into consideration via the
203 Boussinesq approximation [37], which is:

$$(\rho-\rho_0)g=-\rho_0\beta(T-T_0) \tag{7}$$

204 And the momentum equation considering natural convection for PCM is:

$$\frac{\partial\left(\rho u\right)}{\partial t}+\frac{\partial\left(\rho uu\right)}{\partial x}+\frac{\partial\left(\rho uv\right)}{\partial y}=-\frac{\partial \rho}{\partial x}+\frac{\partial}{\partial x}\left(\mu\frac{\partial u}{\partial x}\right)+\frac{\partial}{\partial y}\left(\mu\frac{\partial u}{\partial y}\right)+A_{mush}u \tag{8}$$

$$\frac{\partial\left(\rho v\right)}{\partial t}+\frac{\partial\left(\rho uv\right)}{\partial x}+\frac{\partial\left(\rho vv\right)}{\partial y}=-\frac{\partial \rho}{\partial y}+\frac{\partial}{\partial x}\left(\mu\frac{\partial v}{\partial x}\right)+\frac{\partial}{\partial y}\left(\mu\frac{\partial v}{\partial y}\right)+A_{mush}v+\rho g\alpha\left(T-T_m\right) \tag{9}$$

205 In fact, A_{mush} u and A_{mush} v are momentum dissipation source items, which are used for suppressing velocity in the
206 solid and mushy region. In Eq. (9), the parameter A_{mush} is "porosity function" by Brent et al. [38] definition and it is a
207 constant calculated by Eq.(10) to describe how fast the velocity is decreased to zero when the PCM solidifies.

$$A_{mush}=-C\frac{\left(1-f\right)^2}{f^3+\varepsilon} \tag{10}$$

208 Where $C = 1.0 \times 10^5$ is a mushy zone constant to reflect the melting front morphology, f is local liquid fraction
209 which lies between 0~1 in the mushy zone, and $\varepsilon = 0.001$ is a small number to prevent division by zero. The simulation
210 model has been built in ANSYS/Fluent 14.5.

2.3.2 Initial and boundary conditions

The initial condition for PCM is:

$$t = 0,\ T_{PCM}(x,y) = 298.15K \tag{11}$$

The boundary condition for HTF is:

$$r = r_1,\ T_f = T_{f,in} \tag{12}$$

The boundary condition for the outer wall is:

$$r = r_2,\ \frac{\partial T_{PCM}}{\partial r} = 0 \tag{13}$$

The boundary condition for the inner wall is:

$$u = v = 0,\ r = r_1,\ h_f\left(T_f - T_{PCM}\right) = -\lambda\frac{\partial T_{PCM}}{\partial r} \tag{14}$$

$$h_f = \frac{(\frac{f}{8})\cdot(Re-1000)Pr}{1+12.7\sqrt{\frac{f}{8}}\left(Pr^{\frac{2}{3}}-1\right)}\cdot\frac{k}{2r_1} \tag{15}$$

Where h_f is the forced convection heat transfer coefficient of HTF in the inner tube.

2.3.3 Model validation

Three mesh sizes of 0.5 mm, 0.8 mm and 1 mm are used to identify the grid independence, which is corresponding to the grid number of 6006, 2384 and 1580. **Fig. 3** shows the results of the verification of time step and grid size and the result of using 0.8 mm as mesh size is enough to ensure the accuracy of the numerical calculation, which has no significant change compared with 0.5 mm with a relative deviation of 0.75%. Different time steps, including 0.5 s, 1 s, 2 s, and 5 s, are also considered to ensure that the selected time step does not affect the computational results based on the mesh size of 0.5 mm. The relative deviation of the liquid fraction is small, which is approximately only 0.05%, when the time step is between 0.5 s and 1 s. Based on the verification results, a mesh size of 0.8 mm and a time step of 1s are

used in the subsequent calculation. To meet the convergence criterion, the maximum iterations number in each time step is 400.

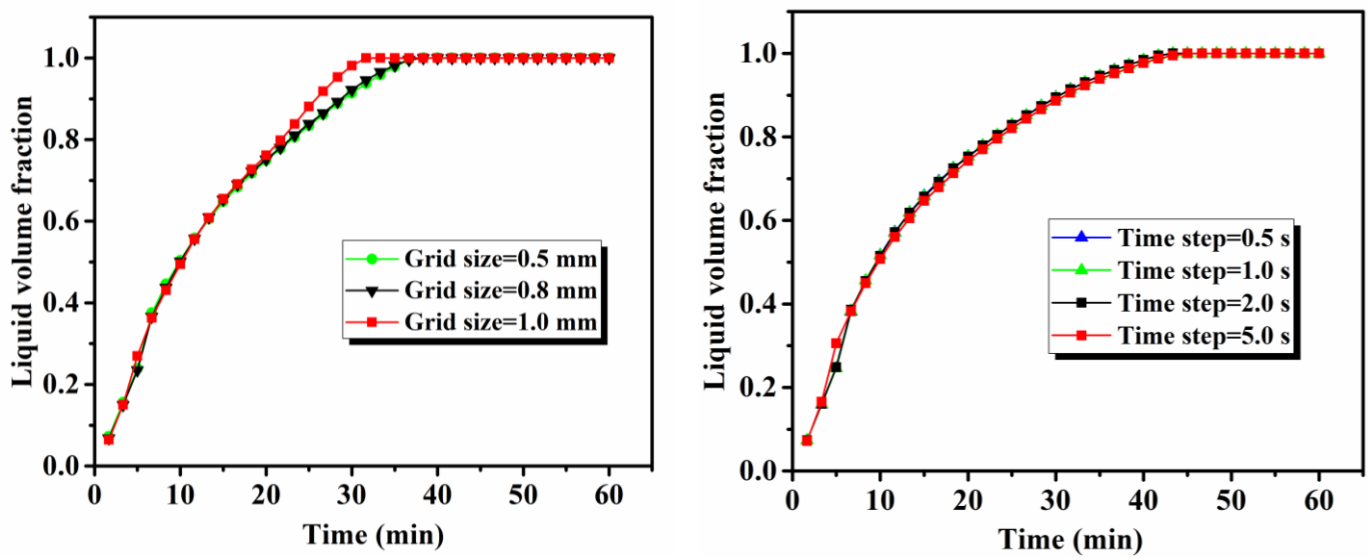

Fig. 3. Validation of the computational time step and grid size: (a) grid size; (b) time step [27].

Under the same conditions, the numerical prediction results are compared with the experimental results from Ref [39] to validate the numerical model shown in **Fig. 4**. In the experimental setup, two thermocouples T_1 and T_2 were placed inside the PCM with the coordinates of (x = 0.51 m, r = 0.002 m) and (x = 0.95 m, r = 0.001 m). The inlet temperature and the mass flow rate of HTF are set at 310.7 K and 0.0315 kg/s, and the initial temperature of PCM takes the value of 282.7 K. It can be seen that the simulated PCM temperature values of the reference points are in close agreement with the experimental values with an error of less than 4.67%. The validation results have proved the precision and reliability of the simulation model.

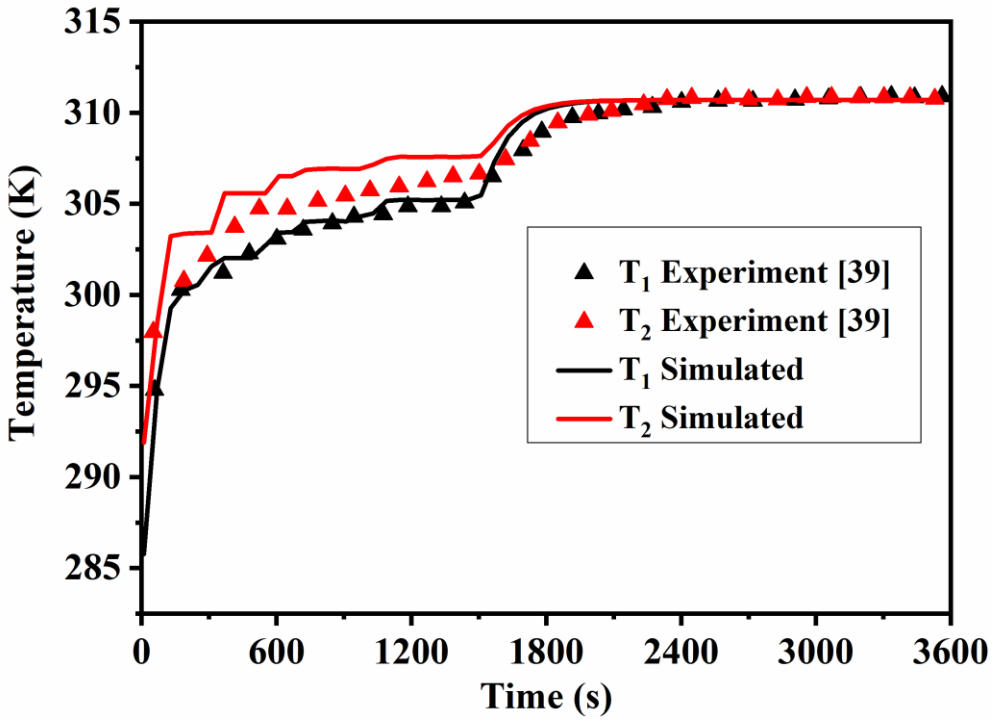

Fig. 4. The simulation model validation results [39].

3. Results and discussion

This section first investigates the influence of the thermophysical properties of PCM on the heat storage performance under steady and fluctuating heat sources, and then conducts the selection study of the actual materials under both conditions. The following table demonstrates the analysis process and the description of methods.

Table 2 The guideline of the conducted tests for the material selection analysis.

Tests	Description
Single-factor effects of PCM thermophysical properties	● Adopt the Orthogonal experiment and range analysis to reveal the single-factor effects of PCM thermophysical properties on LTES performance
Factor interaction effect and prediction	● Consider the factor interaction effect and build the relationships between the objectives and factors by Uniform Design and regression analysis
The ranking of phase change materials	● Based on the two objectives (heat storage capacity and charging rate), use TOPSIS method to rank candidate materials
Results validation	● Conduct the Pareto optimization and the specific simulation study to evaluate and verify the ranking results
Sensitivity analysis of ranking	● Consider different importance degrees of the two objectives

3.1 Single-factor effects of thermophysical properties of PCM

An orthogonal experiment is conducted to investigate how each factor of PCM thermophysical properties affects LTES performance, including density, thermal conductivity, specific heat capacity, latent heat, and melting temperature. The range of each factor depends on the properties of the candidate PCMs. $L_{16}(4^5)$ orthogonal arrays were selected, where L is the mark of the orthogonal table, 16 is line number of orthogonal table, 5 is level of each factor and 4 is column number of the orthogonal table. The designed scheme is shown in **Appendix A**. To reveal the single-factor effects of PCM thermophysical properties, the heat storage capacity at different times and the average charging rate during the melting process were discussed by range analysis. And in range analysis, K_{ij} stands for the average value of the results of each factor and each level, and k_{ij} equals K_{ij} divided by the number of levels and the value of R_j is the difference between maximum average value $k_{j(max)}$ and minimum average value $k_{j(min)}$. The greater the range R is, the larger influence this factor has on the experimental index. Therefore, the magnitude of R can be used to judge the influence of factors.

Fig. 5 demonstrates the relationship between the heat storage capacity with melting time under steady and fluctuating heat source conditions. And under both conditions, the density (ρ) exerts the most significant impact on heat storage capacity among the five factors, followed by the specific heat capacity (C_p), latent heat (L), melting temperature (T_m) and thermal conductivity (λ), i.e., the order is $\rho > C_p > L > T_m > \lambda$. As for steady heat source, the R_Q of density, specific heat capacity and latent heat ascend almost linearly with time. The influence of T_m increases in the first half period, but then decreases gradually during the rest of melting time. On the other hand, the influence of λ is relatively minor among the five factors, but its effect continues to increase with melting time. This is because the initial temperature difference between the heat source and PCM can accelerate the PCM melting at the beginning, while the effect of thermal conductivity will enhance in the last melting process.

As a comparison, the values of R_Q in density and specific heat capacity increase first and then level off around 2000 kJ from 1800 s to 3600 s under fluctuating heat source condition. The reason is that the heat storage capacity reaches

the saturation state in the later melting process, so the effects of ρ and C_p become stable. Additionally, the turning points of λ and T_m appear earlier 900 s than that of the steady heat source, because fluctuating heat source will promote the PCM melting. In general, for storage capacity, there is little difference between the two conditions. The R_Q of specific heat capacity has a slight decline from 1193 kJ to 1131 kJ, so the influence of specific heat capacity is slightly reduced. However, the influence of latent heat is relatively stronger under fluctuating heat source condition compared steady condition.

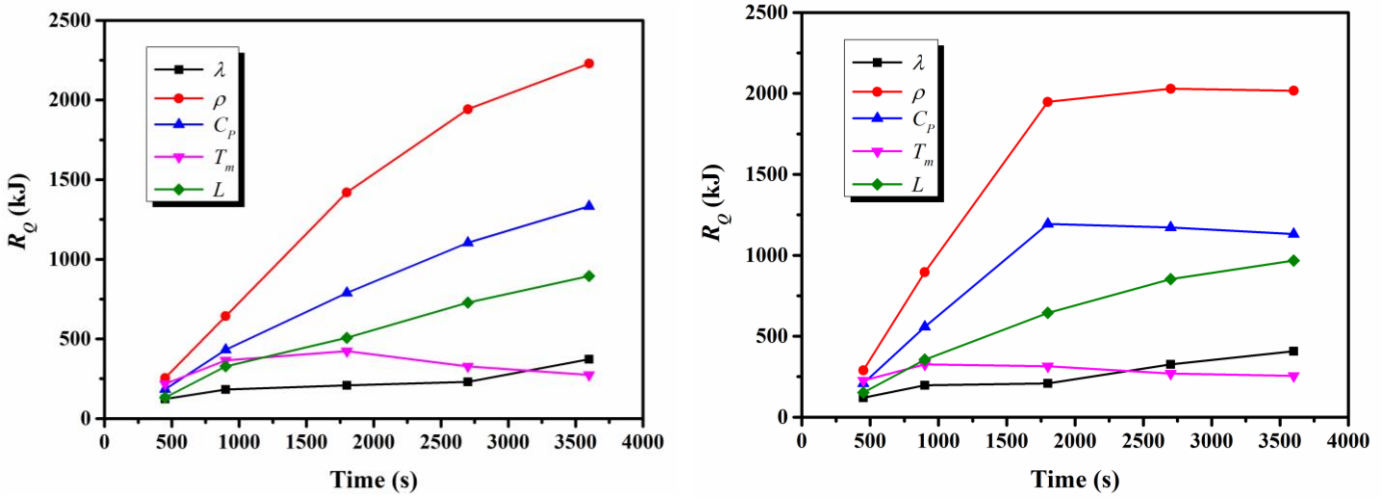

(a) Steady heat source condition (b) Fluctuating heat source condition

Fig. 5. Relationship between heat storage capacity and melting time.

Fig. 6 shows the impact of different PCM thermophysical parameters on the average charging rate of the charging process. Results indicated that the impact order of five factors is $T_m > \lambda > L > C_p > \rho$ for both conditions, but the value difference of R_v between density, specific heat capacity and melting temperature gets closer under fluctuating heat source compared with steady heat source, which indicates that ρ and C_p exert more significant effects on charging rate under fluctuating heat source. The cause might be the temperature fluctuation facilitates the melting process, so the sensible heat mainly takes effect. Although melting temperature and thermal conductivity are not important for heat storage capacity, their effects on the charging rate are highly influential. To further investigate the factor interaction for PCM selection, the detailed relationship between factors and objectives should be established. Therefore, uniform design combined with regression analysis will be conducted in the following section.

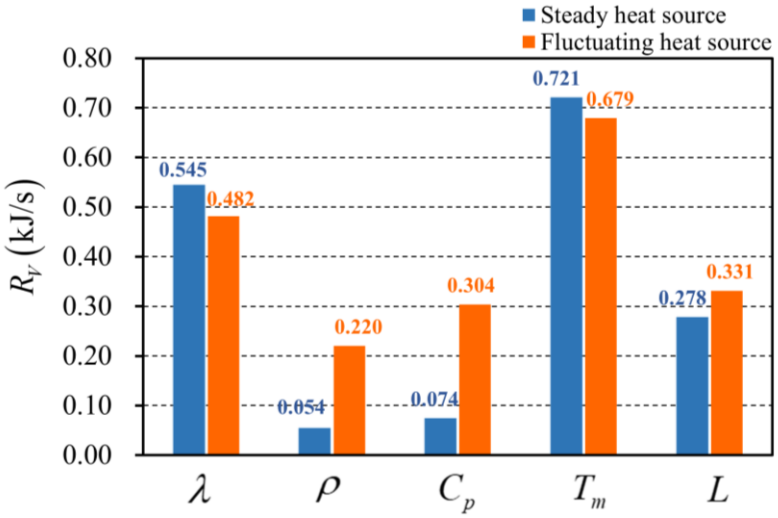

Fig. 6. The impacts of PCM thermophysical properties on the charging rate.

3.2 Factor interaction effect and prediction based on regression analysis

The Uniform Design (UD) method has been developed based on "Probability Theory", "Mathematical Statistics" and "Statistical Experimental Design" as reported in the Ref. [40]. In a uniform design of experiment, experimental trials are uniformly arranged within the designed scopes of investigated parameters. The maximum information is obtained by the uniform design with fewer tests, which is based on the test point "uniform dispersion" [41, 42]. Uniform design tables can be described as $U_n(q^m)$, where U, n, q and m respectively represent the UD, the number of experimental trials, the number of levels and the maximum number of factors. In this work, the five thermophysical parameters are chosen as five variables. Thirty levels for each factor are selected to investigate the influence and interaction of the factors. To improve accuracy, the experiment was carried out using $U_{30}(30^5)$ which was designed by DPS software.

The range of each factor arranged is the same as that in the orthogonal experiment and the guide for using $U_{30}(30^5)$ is listed in **Appendix A**. It is worth noting that the two objectives are heat storage capacity (Q) and charging rate (V). Q represents the heat storage potential of the material. The total charging time is set at 3600 s to ensure that the material can be completely melted, while V denotes the average heat storage rate during the melting process, which takes the effect of the material melting rate into account. Based on the results of UD, it can be observed that Q_{us} is lower than Q_s, but V_{us} is higher than V_s because PCM melts faster as it is affected by the rising temperature in the first half period under fluctuating heat source condition. However, in the second period, due to the drop in the temperature of the fluctuating

heat source, the heat storage of sensible heat is at a disadvantage. To achieve the optimal regression model, which can describe the accurate relationship between the two objectives and these properties parameters, a quadratic polynomial stepwise regression analysis is accomplished by MATLAB. The commonly useful quadratic model is expressed as follows:

$$y = a_0 + \sum_{k=1}^{5} b_k x_k + \sum_{i,j=1}^{5} b_{ij} x_i \, x_j \tag{16}$$

Where b_k and b_{ij} are the unknown values that can be calculated by the simulation data based on the least square method. y indicates the value of the heat storage capacity or charging rate.

The basic idea of stepwise regression is to fit a series of regression equations in order. The latter regression equation is to add or delete an independent variable based on the previous regression equation. Finally, the variables in the regression equation are significant ($p < 0.05$). Regression analysis of Q and V under steady and fluctuating heat source conditions can be represented as the following equations:

$$V_s = 1.151 + 2.196\lambda - 5.347e^{-3}T_m - 2.417e^{-3}\lambda \cdot T_m + 6.886e^{-8}\rho \cdot C_p - 2.14e^{-7}\rho \cdot L - 1.548e^{-6}T_m \cdot L - 0.7482\lambda^2 \quad (R^2=0.996) \tag{17}$$

$$Q_s = 137.061 + 9.576e^{-2}\lambda \cdot \rho + 5.569e^{-4}\rho \cdot C_p + 2.056e^{-3}\rho \cdot L \quad (R^2=0.990) \tag{18}$$

$$V_{us} = 2.429 - 7.986e^{-3}T_m + 1.857e^{-3}L + 7.542e^{-4}\lambda \cdot C_p - 1.731e^{-6}C_p \cdot L \quad (R^2=0.904) \tag{19}$$

$$Q_{us} = 190.639 + 4.937e^{-4}\rho \cdot C_p + 2.149e^{-3}\rho \cdot L - 3.62e^{-4}T_m \cdot C_p \quad (R^2=0.995) \tag{20}$$

The values of R^2 for the heat storage capacity and charging rate show that the second-order polynomial model is significant and fits the data results well. In the multiple regression equation, the partial regression coefficient shows the specific effect of X_j on y_j, but in general, the value of b_k and b_j are affected by the unit of factor. Therefore, the standardization of the partial regression coefficient can directly determine the importance of each regressor to the test result y, which is calculated by Eq. (21). The greater the regression coefficient is, the more important it is to the corresponding factor. The standardised coefficients (P_j) of Eq. (17) - (20) are compared in **Table 3** to analyse which

regressor has a greater impact on the objectives under these two conditions. The values of standard regression coefficients are listed in descending order.

$$P_j = |b_j| \sqrt{\frac{\sum_{j=1}^{m}\left(X_j - \bar{X}_j\right)^2}{\sum_{j=1}^{m}\left(y_j - \bar{y}\right)^2}} \quad j = 1,2,\dots,m;\ b_j = b_k,\ b_{ij};\ X_j = x_k,\ x_i x_j \tag{21}$$

Table 3 Standard regression coefficients of regression expressions.

V_s		Q_s		V_{us}		Q_{us}	
Regressor	P_j	*Regressor*	P_j	*Regressor*	P_j	*Regressor*	P_j
λ	1.523	$\rho \cdot C_p$	0.696	$\lambda \cdot C_p$	0.937	$\rho \cdot C_p$	0.686
λ^2	0.731	$\rho \cdot L$	0.423	$C_p \cdot L$	0.853	$\rho \cdot L$	0.491
T_m	0.556	$\lambda \cdot \rho$	0.050	T_m	0.606	$T_m \cdot C_p$	0.036
$\lambda \cdot T_m$	0.304			L	0.431		
$\rho \cdot C_p$	0.294						
$\rho \cdot L$	0.150						
$T_m \cdot L$	0.081						

Combined with **Table 3** and the positive or negative signs in equations, the results demonstrate that the standard deviation of $\rho \cdot C_p$ is increased by 1 time, and the standard deviation of Q_s is raised by 0.696 times under steady heat source. Therefore, it can be observed that the factors of $\rho \cdot C_p$ and $\rho \cdot L$, which respectively represent sensible heat and latent heat, significantly influence the heat storage capacity Q for either steady and fluctuating heat source conditions. However, the value difference of standard regression coefficients between $\rho \cdot C_p$ and $\rho \cdot L$ is narrowing from 0.273 for steady state to 0.195 for fluctuating state, which means that temperature fluctuation can strengthen the melting process and the effect of latent heat performs more significant. Moreover, $\lambda \cdot \rho$ and $T_m \cdot C_p$ have less impact under steady and fluctuating heat sources respectively. As for the charging rate, the difference between the two conditions is obvious, which is that, for the steady heat source condition, the prominent factor is the thermal conductivity of PCM with λ and λ^2. Combined with the influence direction, it can be seen that the impact of λ on the charging rate gradually rises as a convex function with the increase of λ, and the effect tendency will be weakened as the value of T_m grows

due to the term of $\lambda \cdot T_m$. Additionally, T_m and $\lambda \cdot T_m$ also have a relatively large impact with standard regression coefficients of 0.556 and 0.304. However, for the fluctuating heat source condition, the influence is a relatively complex interaction. The factor with the greatest effect is $\lambda \cdot C_p$ with the highest value of 0.937, followed by $C_p \cdot L$, T_m and L. The general conclusions can also be drawn from **Fig. 5** and **Fig. 6**. In both cases, the density, specific heat capacity and latent heat have a significant effect on heat storage capacity, while for charging rate, the effect of specific heat capacity is more obvious under the fluctuating heat source condition, so the interactions with density and latent heat are also highlighted accordingly. Based on the regression expressions, the heat storage capacity and the charging rate of the candidate materials in both conditions can be obtained. The predictions of heat storage capacity and charging rate are shown in **Table 4**, and the values will be calculated by the TOPSIS method for ranking analysis.

Table 4 List of the predicted results of candidates.

No.	Candidates	$Q_{s\text{-}p}$	$V_{s\text{-}p}$	$Q_{us\text{-}p}$	$V_{us\text{-}p}$
1	KNO_3-$LiNO_3$-$NaNO_3$	2495.548	1.4061	2218.997	1.9336
2	$LiNO_3$-KNO_3	2376.941	1.3044	2121.225	1.8246
3	KNO_3-$NaNO_2$	2575.633	1.3880	2230.498	1.9393
4	KNO_3-$NaNO_3$-$NaNO_2$	2632.751	1.3725	2289.334	1.9139
5	KNO_2-$NaNO_3$	2658.895	1.2565	2330.932	1.7590
6	$LiNO_3$-$NaNO_2$	3824.074	1.3229	3397.633	1.7965
7	$LiNO_3$-$NaNO_3$-KCL	3684.713	1.1734	3322.462	1.6193
8	$LiNO_3$-KCl	3140.030	1.1117	2859.829	1.6217
9	HDPE	1816.058	1.1769	1621.724	1.6291
10	Urea	2442.335	1.3580	2172.606	1.8651
11	HCOONa–HCOOK	1894.811	0.8363	1729.232	1.3686
12	Urea–NH_4Cl	2373.872	1.5833	2124.398	2.1521
13	Urea–NaCl	2407.973	1.5216	2155.234	2.0718
14	Urea–K_2CO_3	2406.618	1.5867	2153.702	2.1605

3.3 Results of ranking using the TOPSIS method

TOPSIS is a Multiple Criteria Decision Making (MCDM) method used for ranking, which has been applied widely across various applications in many fields such as benefit evaluation, health decisions, and health management [43]. TOPSIS can be used to define the relative importance of different factors. The detailed process is presented in **Appendix B**. The ranking results are given in **Fig. 7** by applying equal weighting to the objectives of heat storage capacity and charging rate first. From **Fig. 7** (a) and (b), the top-ranked materials are NO.6, 7, 8, 14 and 12, which are $LiNO_3$-$NaNO_2$, $LiNO_3$-$NaNO_3$-KCL, $LiNO_3$-KCl, Urea–K_2CO_3, and Urea–NH_4Cl. And it is demonstrated that the overall ranking shows no significant difference between steady and fluctuating heat source conditions. This is because NO.6, 7, 8 have an advantage of heat storage capacity, meanwhile, NO. 14 and NO.12 are superior in charging rate under both conditions. Considering the results in **Table 5** and **Fig. 7**, it can be concluded that $LiNO_3$-$NaNO_2$ is ranked as the top one with a significant advantage in comprehensive charging performance having the scores of 0.808 and 0.798 under both steady and fluctuating heat source conditions.

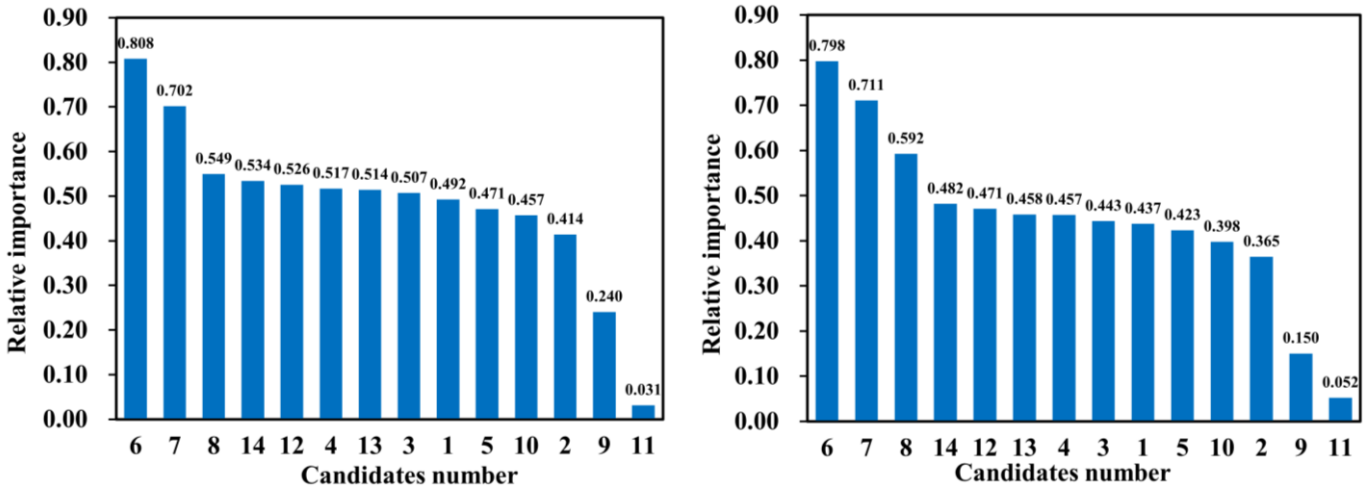

(a) Steady heat source condition (b) Fluctuating heat source condition

Fig. 7. The ranking of selected PCM under steady and fluctuating heat source conditions.

3.4 Validation of ranking results

The MCDM procedure with Pareto optimization can evaluate the ranking results obtained using the TOPSIS method [20]. In Pareto solutions, dominated and non-dominated solutions are distinguished. The non-dominated set of

the entire feasible decision space is called the Pareto-optimal set which consists of optimal values of all the conflicting attributes. The boundary defined by the set of all points mapped from the Pareto optimal set is defined as the Pareto-optimal front. Hence, the results of the fourteen materials are calculated from the two conflict functions, so they can be plotted into one figure to analyse the relative performance of the material. The materials that are closer to the Positive Ideal Solution and furthest from the Negative Ideal Solution are typically more suitable than other materials. The values of the Positive Ideal Solution and the Negative Ideal Solution in the two attributes come from the highest and lowest heat storage capacity and charging rate of all materials.

The materials that are closer to the Positive Ideal Solution and furthest from the Negative Ideal Solution are typically the most suitable choice. The values of the Positive Ideal Solution and the Negative Ideal Solution in the two attributes come from the highest and lowest heat storage capacity and charging rate of all materials. Therefore, the distance from each the Pareto optimal set to the Positive Ideal Solution, which is calculated by $S_i = w_1 \cdot X_p/X_i + w_2 \cdot Y_p/Y_i$ referred from [15]. As shown in **Fig. 8**, the distance values displayed near the corresponding materials number. In this equation, w_1 and w_2 means the weights of the two performance objectives. In this study, equal weights are employed to both objectives. Besides, X_p and Y_p are the coordinate values of the Positive Ideal Solution. As shown, NO.6 and NO.7 has the shortest distance with value of 1.100 and 1.195 under steady heat source. In view of the first front limited to NO.6 or NO.7 material, a second front is proposed by eliminating them from the solution space to verify the remaining materials. For fluctuating heat source condition, NO.6 and NO.7 stay ahead among the materials because of the higher heat storage capacity. Under both conditions, it can be observed that PCMs NO.2, 10, 9, 5, 11 belong to the dominated solution space which consists of weak solutions in both attributes. The top-ranked materials, NO.6, 7, 8, 14, 12 are on the Pareto front which indicates the results obtained from Section 3.3 are aligned well with Pareto optimal solution.

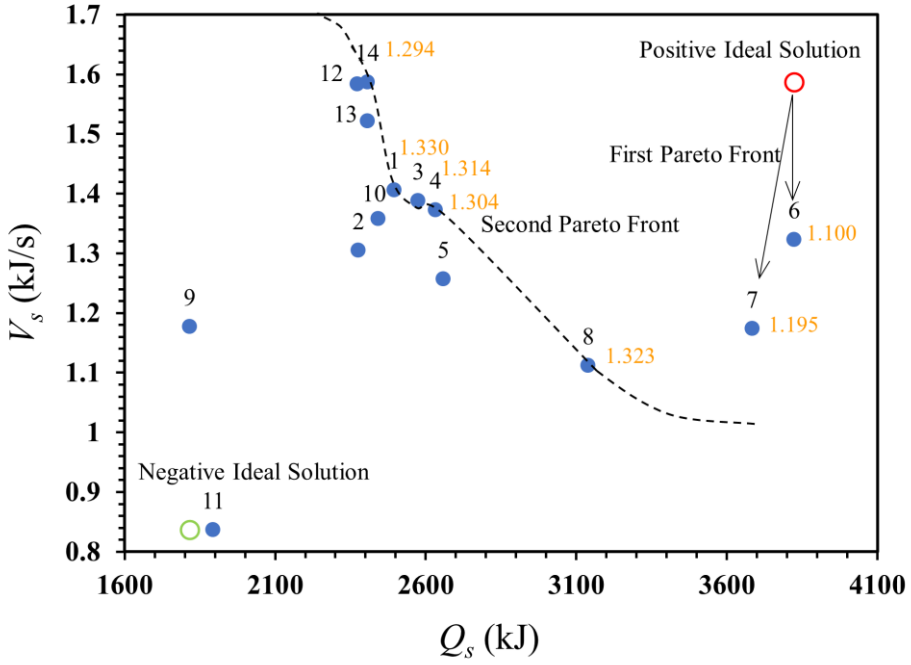

(a) Steady heat source condition

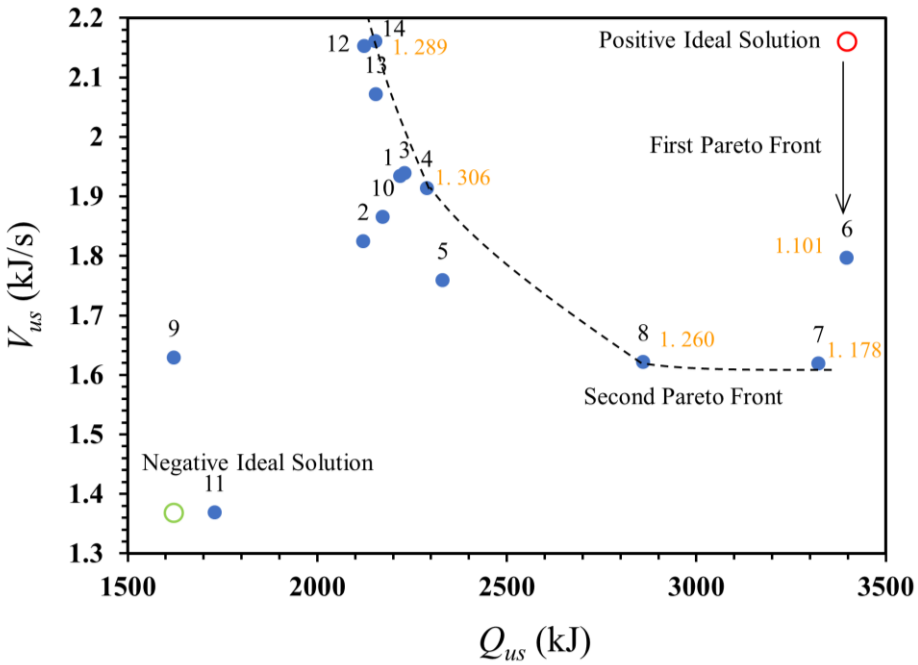

(b) Fluctuating heat source condition

Fig. 8. Examination of materials performance from solution space of attributes.

To further verify the ranking results and analyse the performance of materials in each objective, a simulation study of selected PCM was conducted and the results were plotted in **Fig. 9**. For the comparative analysis, the range normalization of heat storage capacity and charging rate is carried out respectively. Specifically, the linear transformation is shaped to the original data x_i, so that the results are within the range of [0,1] denoted by e, which is a

positive indicator expressed as $e_i = \frac{(x_i - min[xi])}{(max[x_i] - min[xi])}$. **Fig. 9** shows that candidates NO.6, 7, 8 perform better for heat storage capacity, while the candidates NO.14, 12, 13 appear to be excellent in the charging rate and have a stable performance under both conditions, which are in close agreement with the ranking results calculated by TOPSIS method.. Combined with Eq. (17) - (20), it can be proved that candidates NO.12, 13, 14, with the characteristics of low melting temperature and high thermal conductivity and specific heat capacity, can maintain a dominant position for charging rate. Additionally, the variance of e_i for heat storage capacity has no difference between the two conditions, so heat storage capacity can barely be affected by the temperature fluctuation.

As for the charging rate, it can be concluded from Section 3.2 that not only melting temperature and thermal conductivity, but also latent heat and specific heat capacity has a significant influence. However, the impact of latent heat and specific heat capacity will be covered by melting temperature or other factors, so the overall ranking may remain relatively consistent within the selected materials. Just the ranking of three groups demonstrates distinction, which are NO.5 - NO.6 group, NO.3 - NO.1 group, NO.7 - NO.8 group. The reason is that NO.3 and NO.5 have a lower latent heat, which can accelerate the charging rate under fluctuating heat source. For the candidate material NO.8, the effect of specific heat capacity can also be helpful for its charging rate. Besides, it is worth mentioning that the design optimization criteria of materials will be distinctive under the two conditions inferred from Eq. (17-20). Specifically, when the heat source is relatively steady, PCM with greater thermal conductivity, lower melting temperature and an optimal matching for density, specific heat capacity and latent heat can be beneficial for a good comprehensive charging performance of the LTES. When the heat source temperature varies considerably, the requirements of thermal conductivity and melting temperature are the same as under steady heat source, while density is as large as possible, and there is another optimal matching for specific heat capacity and latent heat.

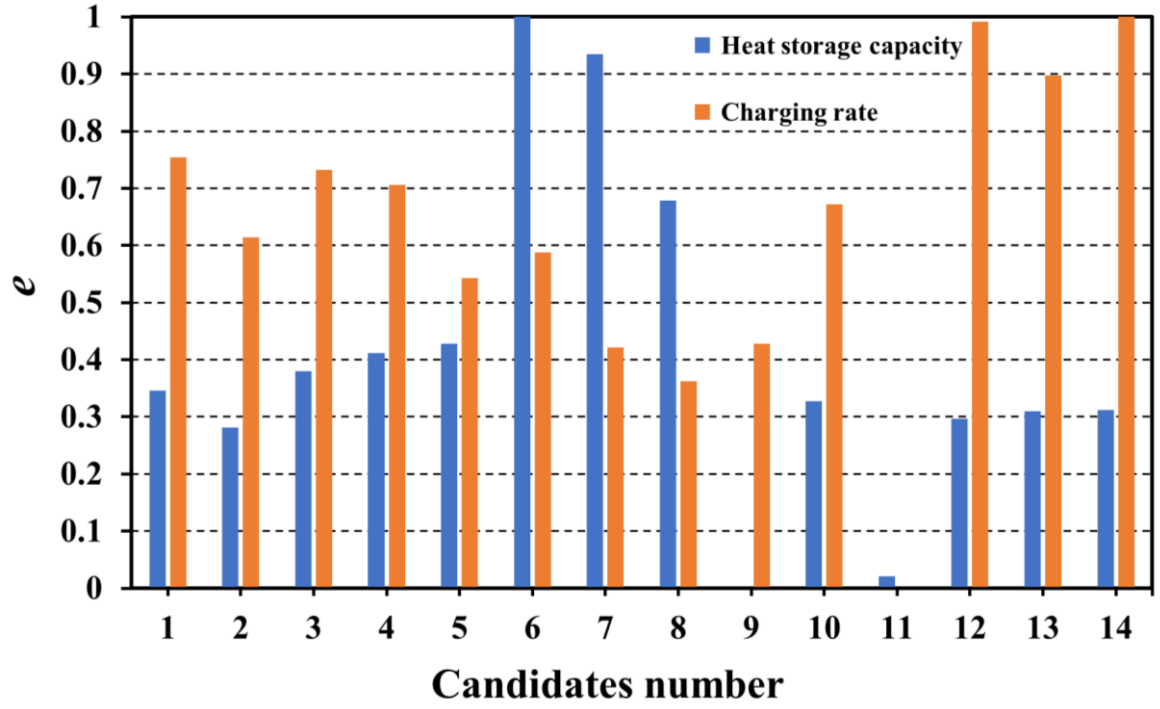

(a) Steady heat source condition

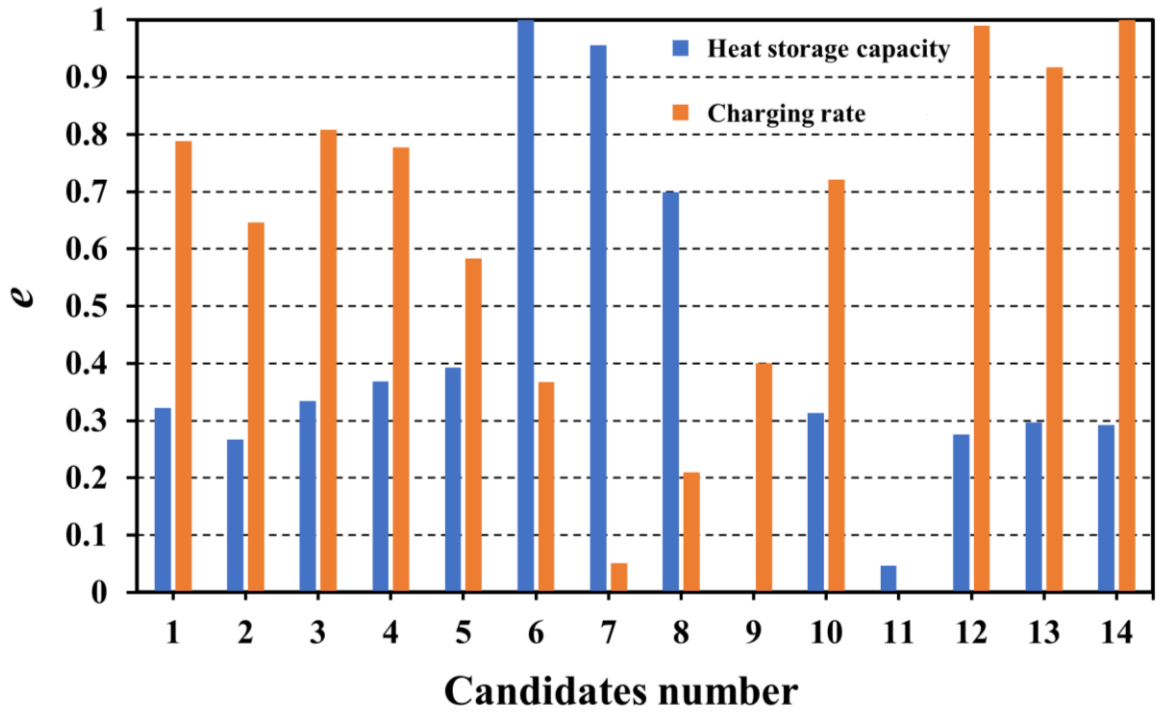

(b) Fluctuating heat source condition

Fig. 9. The normalization simulation results of selected PCM.

3.5 Sensitivity analysis of ranking

Since the two objectives are usually contradictory, a sensitivity analysis is conducted by applying varied weightings to objective expressions as shown in **Table 5**. It can examine the difference in the top five orders under steady and

fluctuating heat source conditions with consideration of different importance degrees of the two indicators. The weightings of heat storage capacity and charging rate are respectively set as 0.1:0.9, 0.3:0.7, 0.5:0.5, 0.7:0.3 and 0.9:0.1. Rs and Rf refers to the ranking under steady heat source and fluctuating heat source respectively. The results indicated that candidate NO.6, which is $LiNO_3$-$NaNO_2$, offers the best comprehensive charging performance under most weighting combinations for both conditions. Besides, the molten salt material has a significant advantage in heat storage capacity, while some Eutectic mixtures with Urea perform better in charging rate, among which Urea–K_2CO_3 is the best. There is no doubt that the definitive selection criteria of materials should be determined according to the specific application, namely the heat storage capacity, the charging rate, or the comprehensive performance of LTES. The ranking results can provide a valuable reference for the selection of PCM in the LTES system.

Table 5 Sensitivity study of ranking under steady and fluctuating heat source conditions.

Weightings ratio	Ranking order	
(Heat storage: Heat-Charging)	Rs	Rf
0.1:0.9	14-12-13-1-3	14-12-13-3-1
0.3:0.7	14-12-6-13-1	6-14-12-13-3
0.5:0.5	6-7-8-14-2	6-7-8-14-2
0.7:0.3	6-7-8-4-5	6-7-8-4-5
0.9:0.1	6-7-8-4-5	6-7-8-4-5

4. Conclusions

This paper has carried out a detailed study on the difference in PCM selection for a shell-and-tube LTES under steady and fluctuating heat source conditions, considering the effects of melting temperature and factor interaction of PCM thermophysical properties. The heat storage capacity and charging rate were taken as objectives to assess the performance of LTES. The parametric study of the LTES performance was investigated under steady and fluctuating heat sources. On the basis, some actual materials with phase change temperatures of 100-200 ℃ were ranked by TOPSIS method and then the verification of ranking results and the sensitivity analysis were performed. Some key findings are concluded as follows:

(1) The primary effects on the heat storage capacity are consistent under both heat source conditions, and the order of prominent factors is the interaction of density and specific heat capacity ($\rho \cdot C_p$), followed by the interaction of density and latent heat ($\rho \cdot L$). As for the charging rate, under the steady heat source condition, the order of key factors is thermal conductivity (λ), followed by melting temperature (T_m). And with the increase of thermal conductivity, its influence on the charging rate rises gradually as a convex function and the effect tendency will be weakened when T_m gets higher. However, under fluctuating heat source condition, the product of the thermal conductivity and specific heat capacity and latent heat of PCM have a significant effect, and the order of prominent factors are $\lambda \cdot C_p$, followed by $C_p \cdot L$.

(2) According to the ranking results, it can be concluded that $LiNO_3$-$NaNO_2$ is the best choice for the heat storage capacity under both heat source conditions, while Urea–K_2CO_3 indicates excellent performance in the charging rate under both conditions due to its lower melting temperature, larger specific heat capacity and thermal conductivity. As a whole, $LiNO_3$-$NaNO_2$ has an attractive comprehensive charging performance for LTES system.

(3) To achieve a better charging performance of LTES comprehensively considering the heat storage capacity and charging rate, PCM design and optimization criteria of PCM are different under steady and fluctuating heat source conditions. For steady heat source conditions, PCM should have greater thermal conductivity, lower melting temperature and an optimal balance among the density, specific heat capacity and latent heat. While the higher density and thermal conductivity and lower melting temperature are preferred and a balance between the specific heat capacity and latent heat should be considered for fluctuating heat sources.

In the future, the optimization of PCMs under different heat source conditions should be investigated, and the quantitative results of PCM optimal thermophysical properties can be obtained and analysed. In addition, the coupling effect between materials and the geometric parameters of LTES systems should be considered together. Furthermore, more dynamic heat sources and a wider melting temperature range of PCM will be further investigated for extending

449 the scope of this study, digging deeper into the regularity of the influence of dynamic fluctuations of heat sources on
450 PCM selection.

451 Credit authorship contribution statement

452 **Xiaoli Yu:** Conceptualization, Methodology, Investigation, Validation, Funding acquisition. **Jinwei Chang:** Writing-
453 Original draft preparation, Methodology, Formal analysis. **Rui Huang:** Supervision, Project administration, Resources.
454 **Yan Huang:** Formal analysis, Data curation. **Yiji Lu:** Writing- Reviewing and Editing, Supervision. **Zhi Li:**
455 Conceptualization, Writing- Reviewing and Editing. **Lei Wang:** Funding acquisition, Project administration, Resources.

456 Acknowledgements

457 The research project has been funded by the National Natural Science Foundation of China (Grant No. 51976176 and
458 No. 51806189). Support from the China Science Foundation (Grant No. 2018M640556 and 2019T120514), from
459 Zhejiang Province Science Foundation (Grant No. ZJ20180099) and from the Fundamental Research Funds for the
460 Central Universities (Grant No. 2020QNA4008) are also greatly appreciated. The authors also would like to thank the
461 Royal Academy of Engineering through the Transforming Systems through Partnerships programme (Grant No.
462 TSPC1098).

463

Appendix A. Supplementary Tables

Table A.1 The orthogonal experiment design $L_{16}(4^5)$.

No.	λ	ρ	C_p	T_m	L
1	1	2500	2400	190	370
2	1	1900	1800	160	275
3	1	1400	1350	130	185
4	1	900	900	100	95
5	0.7	2500	1800	130	95
6	0.7	1900	2400	100	185
7	0.7	1400	900	190	275
8	0.7	900	1350	160	370
9	0.5	2500	1350	100	275
10	0.5	1900	900	130	370
11	0.5	1400	2400	160	95
12	0.5	900	1800	190	185
13	0.4	2500	900	160	185
14	0.4	1900	1350	190	95
15	0.4	1400	1800	100	370
16	0.4	900	2400	130	275

Table A.2 Uniform design table of $U_{30}(30^5)$ and simulation results.

No.	λ	ρ	C_p	T_m	L	Q_s	V_s	Q_{us}	V_{us}
1	0.71	1783	1883	190	275	3160.59	1.025	2817.75	1.471
2	0.48	1672	1003	171	142	1599.06	0.954	1427.85	1.524
3	0.75	2279	1055	162	304	3097.38	1.173	2838.51	1.732
4	0.59	1562	1676	153	370	2966.34	1.144	2678.10	1.655
5	0.79	1617	2090	100	209	2895.75	1.837	2516.37	2.552
6	0.67	1010	1262	174	342	1588.80	0.986	1480.08	1.575
7	0.69	1948	2400	112	180	3673.96	1.724	3202.76	2.444
8	0.81	1728	1469	134	361	3028.41	1.440	2745.04	2.114
9	0.57	1286	1521	187	190	1784.85	0.938	1575.96	1.562
10	0.42	2114	2038	159	161	3354.24	1.088	2955.99	1.352
11	0.63	1452	2193	147	114	2367.70	1.398	2010.09	2.086
12	0.44	1341	1159	125	218	1663.01	1.157	1501.55	1.677
13	0.73	900	1417	119	152	1106.26	1.518	997.76	1.935
14	0.61	2059	900	116	266	2443.18	1.384	2248.15	1.993
15	0.65	2500	1728	131	247	4033.20	1.457	3605.75	1.937
16	0.86	2224	2245	122	351	4751.08	1.681	4285.44	2.192
17	0.52	955	2297	137	237	1898.27	1.241	1654.82	1.838
18	0.98	1838	1934	128	133	2776.05	1.787	2377.81	2.533
19	0.40	1893	1314	143	285	2810.21	1.020	2532.69	1.382
20	0.92	2445	1366	150	199	3193.64	1.475	2824.18	2.217
21	0.96	1507	1107	106	313	2126.81	1.715	1969.13	2.352
22	0.83	2169	1210	184	123	2278.54	1.186	1981.63	1.926
23	0.90	1397	2348	181	256	2852.25	1.234	2488.30	1.966
24	0.54	2334	1572	103	104	2860.89	1.649	2459.60	2.337
25	0.77	1231	1779	165	95	1634.45	1.342	1397.06	1.955
26	0.50	2390	2141	178	323	4311.13	0.989	3975.65	1.111
27	0.94	1066	1986	156	294	2040.68	1.383	1816.40	2.069
28	0.88	1121	952	140	171	1099.18	1.408	1021.59	1.859
29	0.46	1176	1831	109	332	2272.06	1.301	2030.42	1.870
30	1.00	2003	1624	168	228	3066.99	1.363	2705.08	2.119

Appendix B. Techniques for Older Preference by Similarity to Ideal Solutions (TOPSIS) method [15]

The principle of TOPSIS is that the alternatives chosen should be as close to the ideal solution as possible and as far

away from the negative ideal solution as possible. For each attribute, the ideal solution is from a combination of the best performance values in the decision matrix, while the negative ideal solution is from a combination of the worst performance values. The mathematical steps of TOPSIS are as follows:

Step 1: Construct decision matrix $A = (a_{ij})_{m\times n}$ of project evaluation which consists of n number of attribute values for m numbers of alternatives. To get rid of the dimensional effect, $B = (b_{ij})_{m\times n}$ is obtained through normalized processing.

$$b_{ij} = \frac{a_{ij}}{\sqrt{\sum_{i=1}^{m} a_{ij}^2}}, \quad i = 1, \cdots, m, \; j = 1, \cdots, n \tag{A.1}$$

Step 2: According to the contribution of each evaluation index to the evaluation results, different weightings are assigned: $w = [w_1, \cdots, w_n]$. The j_{th} column of B is multiplied by its weighting w_j to obtain the weighted normalized matrix $C = (c_{ij})_{m\times n}$

Step 3: Determine the positive ideal solutions C^* and negative ideal solutions C^0

$$C^* = [c_1^*, \cdots, c_n^*], \quad C^0 = [c_1^0, \cdots, c_n^0] \tag{A.2}$$

Where

$$c_j^* = \begin{cases} \max\limits_i c_{ij} \\ \min\limits_i c_{ij} \end{cases}, \; c_j^0 = \begin{cases} \min\limits_i c_{ij} \\ \max\limits_i c_{ij} \end{cases}, \; j = 1, \cdots, n \tag{A.3}$$

Step 4: Calculate the distance from each alternative to the positive and negative ideal solutions.

$$d_i^* = \sqrt{\sum_{j=1}^{n} (c_{ij} - c_j^*)^2}, \quad i = 1, \cdots, m \tag{A.4}$$

$$d_i^0 = \sqrt{\sum_{j=1}^{n} (c_{ij} - c_j^0)^2}, \quad i = 1, \cdots, m \tag{A.5}$$

Step 5: Compute the relative importance of each alternative to the ideal solution with the Euclidean distance equation. Finally, arrange f_i in descending order to obtain the relative importance of each evaluation alternative.

$$f_i = \frac{d_i^0}{d_i^0 + d_i^*}, \quad i = 1, \cdots, m \tag{A.6}$$

486

Reference

[1] G. Liu, J. Liu, J. E, Y. Li, Z. Zhang, J. Chen, X. Zhao, W. Hu, Effects of different sizes and dispatch strategies of thermal energy storage on solar energy usage ability of solar thermal power plant, Applied Thermal Engineering, 156 (2019) 14-22.

[2] H. Wang, W. Lu, Z. Wu, G. Zhang, Parametric analysis of applying PCM wallboards for energy saving in high-rise lightweight buildings in Shanghai, Renewable Energy, 145 (2020) 52-64.

[3] J. Song, C.-w. Gu, X. Ren, Parametric design and off-design analysis of organic Rankine cycle (ORC) system, Energy Conversion and Management, 112 (2016) 157-165.

[4] C. Prieto, L.F. Cabeza, Thermal energy storage (TES) with phase change materials (PCM) in solar power plants (CSP). Concept and plant performance, Applied Energy, 254 (2019) 113646.

[5] H. Jafari Mosleh, R. Ahmadi, Linear parabolic trough solar power plant assisted with latent thermal energy storage system: A dynamic simulation, Applied Thermal Engineering, 161 (2019) 114204.

[6] M. Esen, Thermal performance of a solar-aided latent heat store used for space heating by heat pump, Solar Energy, 69 (2000) 15-25.

[7] M. Faegh, M.B. Shafii, Experimental investigation of a solar still equipped with an external heat storage system using phase change materials and heat pipes, Desalination, 409 (2017) 128-135.

[8] X. Li, J. Song, G. Yu, Y. Liang, H. Tian, G. Shu, C.N. Markides, Organic Rankine cycle systems for engine waste-heat recovery: Heat exchanger design in space-constrained applications, Energy Conversion and Management, 199 (2019).

[9] Y. Lu, A.P. Roskilly, X. Yu, K. Tang, L. Jiang, A. Smallbone, L. Chen, Y. Wang, Parametric study for small scale engine coolant and exhaust heat recovery system using different Organic Rankine cycle layouts, Applied Thermal Engineering, 127 (2017) 1252-1266.

[10] L. Cioccolanti, R. Tascioni, A. Arteconi, Mathematical modelling of operation modes and performance evaluation of an innovative small-scale concentrated solar organic Rankine cycle plant, Applied Energy, 221 (2018) 464-476.

[11] F. Dal Magro, M. Jimenez-Arreola, A. Romagnoli, Improving energy recovery efficiency by retrofitting a PCM-based technology to an ORC system operating under thermal power fluctuations, Applied Energy, 208 (2017) 972-985.

[12] M. Esen, T. Ayhan, Development of a model compatible with solar assisted cylindrical energy storage tank and variation of stored energy with time for different phase change materials, Energy Conversion and Management, 37 (1996) 1775-1785.

[13] C. Nie, J. Liu, S. Deng, Effect of geometry modification on the thermal response of composite metal foam/phase change material for thermal energy storage, International Journal of Heat and Mass Transfer, 165 (2021) 120652.

[14] M. Esen, A. Durmuş, A. Durmuş, Geometric design of solar-aided latent heat store depending on various parameters and phase change materials, Solar Energy, 62 (1998) 19-28.

[15] H. Xu, A. Romagnoli, J.Y. Sze, X. Py, Application of material assessment methodology in latent heat thermal energy storage for waste heat recovery, Applied Energy, 187 (2017) 281-290.

[16] J.Z. Alvi, Y. Feng, Q. Wang, M. Imran, J. Alvi, Modelling, simulation and comparison of phase change material storage based direct and indirect solar organic Rankine cycle systems, Applied Thermal Engineering, 170 (2020) 114780.

[17] X. Yu, Z. Li, Y. Lu, R. Huang, A.P. Roskilly, Investigation of organic Rankine cycle integrated with double latent thermal energy storage for engine waste heat recovery, Energy, 170 (2019) 1098-1112.

[18] S.-Z. Tang, Y. He, Y.-L. He, F.-L. Wang, Enhancing the thermal response of a latent heat storage system for suppressing temperature fluctuation of dusty flue gas, Applied Energy, 266 (2020).

[19] A. Loganathan, I. Mani, A fuzzy based hybrid multi criteria decision making methodology for phase change material selection in electronics cooling system, Ain Shams Engineering Journal, 9 (2018) 2943-2950.
[20] M. Rastogi, A. Chauhan, R. Vaish, A. Kishan, Selection and performance assessment of Phase Change Materials for heating, ventilation and air-conditioning applications, Energy Conversion and Management, 89 (2015) 260-269.
[21] W. Tang, Z. Wang, E. Mohseni, S. Wang, A practical ranking system for evaluation of industry viable phase change materials for use in concrete, Construction and Building Materials, 177 (2018) 272-286.
[22] X. Yang, P. Wei, X. Wang, Y.-L. He, Gradient design of pore parameters on the melting process in a thermal energy storage unit filled with open-cell metal foam, Applied Energy, 268 (2020).
[23] Y. Li, S. Liu, J. Lu, Effects of various parameters of a PCM on thermal performance of a solar chimney, Applied Thermal Engineering, 127 (2017) 1119-1131.
[24] Y.B. Tao, V.P. Carey, Effects of PCM thermophysical properties on thermal storage performance of a shell-and-tube latent heat storage unit, Applied Energy, 179 (2016) 203-210.
[25] Y. Huo, J. Zong, Z. Rao, The investigations on the heat transfer in thermal energy storage with time-dependent heat flux for power plants, Energy, 175 (2019) 1209-1221.
[26] Z. Li, Y. Lu, R. Huang, L. Wang, R. Jiang, X. Yu, X. Yu, Parametric study on melting process of a shell-and-tube latent thermal energy storage under fluctuating thermal conditions, Applied Thermal Engineering, 180 (2020).
[27] Z. Li, X. Yu, L. Wang, Y. Lu, R. Huang, J. Chang, R. Jiang, Effects of fluctuating thermal sources on a shell-and-tube latent thermal energy storage during charging process, Energy, 199 (2020) 117400.
[28] S. Seddegh, X. Wang, M.M. Joybari, F. Haghighat, Investigation of the effect of geometric and operating parameters on thermal behavior of vertical shell-and-tube latent heat energy storage systems, Energy, 137 (2017) 69-82.
[29] R. Anish, V. Mariappan, M. Mastani Joybari, Experimental investigation on the melting and solidification behavior of erythritol in a horizontal shell and multi-finned tube latent heat storage unit, Applied Thermal Engineering, 161 (2019).
[30] Y. Wang, L. Wang, N. Xie, X. Lin, H. Chen, Experimental study on the melting and solidification behavior of erythritol in a vertical shell-and-tube latent heat thermal storage unit, International Journal of Heat and Mass Transfer, 99 (2016) 770-781.
[31] Y.B. Tao, Y.K. Liu, Y.-L. He, Effects of PCM arrangement and natural convection on charging and discharging performance of shell-and-tube LHS unit, International Journal of Heat and Mass Transfer, 115 (2017) 99-107.
[32] C. Hwang, K. Yoon, Multiple attribute decision making: methods and applications, A state of the art survey, New York: Springer-Verlag (1981).
[33] H. Huang, Y. Xiao, J. Lin, T. Zhou, Y. Liu, Q. Zhao, Improvement of the efficiency of solar thermal energy storage systems by cascading a PCM unit with a water tank, Journal of Cleaner Production, 245 (2020) 118864.
[34] M.K. Rathod, J. Banerjee, Thermal stability of phase change materials used in latent heat energy storage systems: A review, Renewable and Sustainable Energy Reviews, 18 (2013) 246-258.
[35] J. Pereira da Cunha, P. Eames, Thermal energy storage for low and medium temperature applications using phase change materials – A review, Applied Energy, 177 (2016) 227-238.
[36] Y.B. Tao, Y.L. He, Effects of natural convection on latent heat storage performance of salt in a horizontal concentric tube, Applied Energy, 143 (2015) 38-46.
[37] A.A. Al-Abidi, S. Mat, K. Sopian, M.Y. Sulaiman, A.T. Mohammad, Numerical study of PCM solidification in a triplex tube heat exchanger with internal and external fins, International Journal of Heat and Mass Transfer, 61 (2013) 684-695.
[38] A.D. Brent, V.R. Voller, K.J. Reid, Enthalpy-porosity technique for modeling convection-diffusion phase

change: application to the melting of a pure metal, Numerical Heat Transfer, 13 (1988) 297-318.
[39] M. Lacroix, Numerical simulation of a shell and tube latent thermal energy storage unit, Sol Energy, 50 (1993) 357–367.
[40] K. Fang, Y. Wang, Number-theoretic methods in statistics, 1st ed., Chapman & Hall, London ; New York, 1994.
[41] Q. Xiong, Z. Li, H. Luo, Z. Zhao, Wind tunnel test study on wind load coefficients variation law of heliostat based on uniform design method, Solar Energy, 184 (2019) 209-229.
[42] J.F. Li, H.L. Liao, C.X. Ding, C. Coddet, Optimizing the plasma spray process parameters of yttria stabilized zirconia coatings using a uniform design of experiments, Journal of Materials Processing Technology, 160 (2005) 34-42.
[43] K. Yang, N. Zhu, C. Chang, D. Wang, S. Yang, S. Ma, A methodological concept for phase change material selection based on multi-criteria decision making (MCDM): A case study, Energy, 165 (2018) 1085-1096.